

Millimeter Wave MIMO Prototype: Measurements and Experimental Results

Vasanthan Raghavan, Andrzej Partyka, Ashwin Sampath, Sundar Subramanian,
Ozge Hizir Koymen, Kobi Ravid, Juergen Cezanne, Kiran Mukkavilli, Junyi Li

Abstract

Millimeter-wave multi-input multi-output (mm-Wave MIMO) systems are one of the candidate schemes for 5G wireless standardization efforts. In this context, the main contributions of this article are three-fold. 1) We describe parallel sets of measurements at identical transmit-receive location pairs with 2.9, 29 and 61 GHz carrier frequencies in indoor office, shopping mall, and outdoor settings. These measurements provide insights on propagation, blockage and material penetration losses, and the key elements necessary in system design to make mm-Wave systems viable in practice. 2) One of these elements is hybrid beamforming necessary for better link margins by reaping the array gain with large antenna dimensions. From the class of fully-flexible hybrid beamformers, we describe a robust class of directional beamformers towards meeting the high data-rate requirements of mm-Wave systems. 3) Leveraging these design insights, we then describe an experimental prototype system at 28 GHz that realizes high data-rates on both the downlink and uplink and robustly maintains these rates in outdoor and indoor mobility scenarios. In addition to maintaining large signal constellation sizes in spite of radio frequency challenges, this prototype leverages the directional nature of the mm-Wave channel to perform seamless beam switching and handover across mm-Wave base-stations thereby overcoming the path losses in non-line-of-sight links and blockages encountered at mm-Wave frequencies.

Index Terms

Millimeter-wave, experimental prototype, MIMO, channel measurements, beamforming, handover, RF.

I. INTRODUCTION

Millimeter-wave multi-input multi-output (mm-Wave MIMO) systems are one of the candidates for the physical layer (PHY) in the currently ongoing standardization efforts for the Fifth

The authors are with Qualcomm Corporate R&D, Bridgewater, NJ 08807, USA and Qualcomm Corporate R&D, San Diego, CA 92121, USA.

Generation (5G) air link specifications. Over the last few years, there has been an exploding interest on mm-Wave systems (see, e.g., [1]–[3] and references therein). Most of these works either present expectations from mm-Wave systems, or use-case analysis, or channel measurements, or performance studies assuming certain PHY abstractions. With this backdrop, the focus of this paper is on understanding the implementation of mm-Wave systems in practice and to present a complete picture starting from channel measurements to system design implications to prototype performance.

Towards this goal, we first study electromagnetic propagation in the mm-Wave regime using a number of parallel measurements at the *same* transmit-receive location pairs in different use-cases (indoor office, shopping mall and outdoor) at 2.9, 29 and 61 GHz. Such a parallel set of measurements minimizes the number of confounding factors and allows a direct comparison of propagation across different carrier frequencies. A limited number of such measurement studies at the same location pairs are available in the literature. While our studies show that losses at mm-Wave frequencies are typically higher than with sub-6 GHz systems, these losses are not substantially worse. Nevertheless, additional losses due to hand/human blockages and material penetration can be significantly detrimental to the link margins and are expected to play the role of a serious differentiator for a mm-Wave chipset solution.

The above observations motivate the use of beamforming to overcome these losses. We then briefly describe the radio frequency (RF) component challenges that impact the design of a practical mm-Wave chipset. The use of near-optimal beamforming structures needed to improve the link margin in both single- and multi-user contexts in a practical mm-Wave chipset is not viable due to cost and complexity challenges of radio frequency (RF) components. Thus, secondly, to overcome these constraints, we are motivated to use a certain subset of *directional* beamformers for MIMO transmissions. In addition to low complexity, the proposed approaches also enjoy advantages such as robustness to phase changes across paths (an issue of immense importance for small wavelength systems such as mm-Wave) and a simpler system design for initial user equipment (UE) discovery and subsequent beam refinement.

With this background, thirdly, we describe our prototype system operating at 28 GHz that realizes a robust directional beamforming solution leading to high data-rates on both the downlink and uplink. We describe various experiments performed with the prototype in both outdoor and indoor scenarios and provide unique insights into the operations of a practical mm-Wave system.

The key elements tested by these experiments include robustness of mm-Wave links in non-line-of-sight (NLOS) settings via beam switching in response to mobility and blockage, inter-base-station handover, and interference management. Comparable prototypes in the literature such as [4] mostly emphasize peak throughputs in line-of-sight (LOS) settings and do not provide lessons applicable for practical deployments. Other prototypes of importance in practical deployments include the CAP-MIMO architecture [5] and [6]–[8] that apply lens array techniques for steering multiple beams from the base-station.

II. MILLIMETER-WAVE CHANNEL MEASUREMENTS AND SYSTEM IMPLICATIONS

The focus of this section is on reporting mm-Wave channel measurements at 2.9, 29 and 61 GHz, which are representative of the three most-likely commercial offerings in the 2018-20 time-frame and likely to be compared against each other in terms of performance: sub-6 GHz 5G-NR, mm-Wave MIMO 5G-NR, and 802.11ad/ax/ay. While a number of mm-Wave channel measurement campaigns have been reported in the literature, the novelty of this work is on channel propagation comparisons across these three carrier frequencies at *identical* transmit-receive location pairs in different use-cases. Such studies are important as they eliminate most confounding factors that prevent a direct comparison across frequencies.

Towards this goal, channel sounding is performed with both omni-directional antennas as well as directional horn antennas. For directional measurements, an azimuthal scan (or a 360° view) with a 10 dBi gain horn antenna and producing 39 directional slices, and a spherical scan (360° azimuth view and -30° to 90° view in elevation) with a 20 dBi gain horn antenna and producing 331 directional slices are generated. The time-resolution of the channel sounder is approximately 5 ns. An Agilent E8267D signal generator is used to generate a pseudo-noise (PN) sequence at a chip rate of 100 Mc/s, which is then used to sound the channel. At the receiver, an Agilent N9030A signal analyzer is used for acquisition and the PN chip sequence is despread using a sampler at 200 MHz and with 16 bit resolution.

These sounding measurements are obtained for the indoor office setting (two floors of the Qualcomm building in Bridgewater, NJ), indoor shopping mall setting (Bridgewater Commons Mall, Bridgewater, NJ), outdoor settings (open areas outside the Qualcomm building), including the suburban setting (residential location in Bedminster, NJ) and the Urban Micro setting (New Brunswick, NJ), etc., as well as emulation of stadium deployments. These measurement scenarios

are representative of typical applications considered for future deployment efforts.

While macroscopic channel properties such as path loss are studied with omni-directional scans, other properties such as delay spread, path diversity, etc., are studied with both omni-directional and directional scans. Processing of these measurements lead to the following observations and implications on system design for mm-Wave channels. More technical details on these studies can be found in [9].

Path Loss: Measurements in different deployments are used to study macroscopic properties of LOS and NLOS links. We use a frequency-dependent path loss model with a close-in free space reference distance of $d_0 = 1$ m where the path loss (in dB) at a distance of d m is modeled as

$$\text{PL}(d) = \text{PL}(d_0) + \alpha \cdot 10 \log_{10}(d/d_0) + \mathsf{X}, \quad \mathsf{X} \sim \mathcal{N}(0, \sigma_{\mathsf{X}}^2). \quad (1)$$

The path loss exponents (PLEs), denoted as α , and the shadowing factors (σ_{X}) for different types of links (LOS/NLOS) in different use-cases are learned with a least-squares fitting of the model in (1) to the measured data. These parameters are listed in Table I and they show that PLEs and shadowing factors for NLOS links generally increase with frequency. For LOS links, PLEs are generally smaller than those for NLOS links and in indoor settings can be smaller than the freespace PLE of 2. A plausible explanation for this observation is *waveguide effect* where long enclosures such as walkways/corridors, dropped/false ceilings, etc., tend to propagate electromagnetic energy via alternate modes/more reflective paths decreasing the PLE. Shadowing factors show inconsistent behavior with frequency. From Table I, we conclude that while mm-Wave systems experience higher path losses than sub-6 GHz systems, the differential impact of the PLEs and shadowing factors on link margin at higher carrier frequencies is *not* dramatic.

Delay Spread: The delay spread of the channel is an important metric to understand the system overhead (in terms of the cyclic prefix length for a multi-carrier design). In this context, frequency-dependent delay spreads are observed in NLOS settings both with omni-directional and directional antennas. While omni-directional delay spreads are small in most scenarios (for example, the essential spread is on the order of 30-50 ns in indoor office, 50-90 ns in indoor shopping mall and 150-300 ns in outdoor street canyon settings), there are also scenarios where a significantly large delay spread is seen (e.g., even up to 800 ns in outdoor open square settings). These extreme scenarios can be explained with the *radar cross-section effect*, where seemingly small objects that do not participate in electromagnetic propagation at lower frequencies show

TABLE I
PATH LOSS MODEL PARAMETERS IN DIFFERENT USE-CASES

Parameter ↓	LOS			NLOS			LOS			NLOS		
f_c (in GHz) →	2.9	29	61	2.9	29	61	2.9	29	61	2.9	29	61
	Indoor office						Indoor shopping mall					
PLE (α)	1.62	1.46	1.59	3.08	3.46	4.17	1.93	1.98	2.05	2.61	2.76	2.98
σ_x (in dB)	5.49	4.25	4.81	6.60	8.31	13.83	5.32	3.56	4.29	9.08	9.47	12.86
	Urban Micro street canyon						Outdoor open areas					
PLE (α)	2.18	2.19	2.22	2.95	3.07	3.27	2.41	2.73	2.83	3.01	3.39	3.42
σ_x (in dB)	4.41	4.37	4.84	7.82	8.16	10.70	4.60	5.73	6.78	4.00	8.03	1.97

up at higher frequencies. Such behavior happens as the wavelength approaches the roughness of surfaces (e.g., walls, light poles, etc.). Supporting these extremes without incurring a high fixed system overhead is important. In most indoor scenarios, sparse scattering implies that the beamformed delay spread is comparable with the omni-directional delay spread. While the same trend holds for most scenarios in the outdoor setting, the beamformed delay spread can be significantly smaller than the omni-directional delay spread for the tail values.

Blockage: An important feature that makes mm-Wave propagation significantly different from propagation at sub-6 GHz frequencies is that a large area of the UE can be easily covered and blocked by parts of the human body, other humans, vehicles, foliage, etc. Additional link impairments due to these blockers (not seen at sub-6 GHz) are observed at mm-Wave frequencies and the practical viability of mm-Wave systems are more dependent on blockage than the path losses reported in Table I. For example, a typical UE design with multiple linear subarray units of four antenna elements (on the Top and Long edges of the device) is presented for the Landscape mode in Fig. 1(a). Corresponding to this UE antenna design, Figs. 1(b)-(d) show the received gain in azimuth and elevation in Freespace, and with hand blocking in the Landscape and Portrait modes, respectively. While almost the entire sphere is covered around the UE in the Freespace mode, the presence of hand leads to an angular blockage region of $160^\circ \times 75^\circ$ (blue areas) in the Landscape mode. The region in blue stretches from behind the palm to the thumb. In this setting, the Top edge subarray is not useful and the Long edge subarray allows good signal reception.

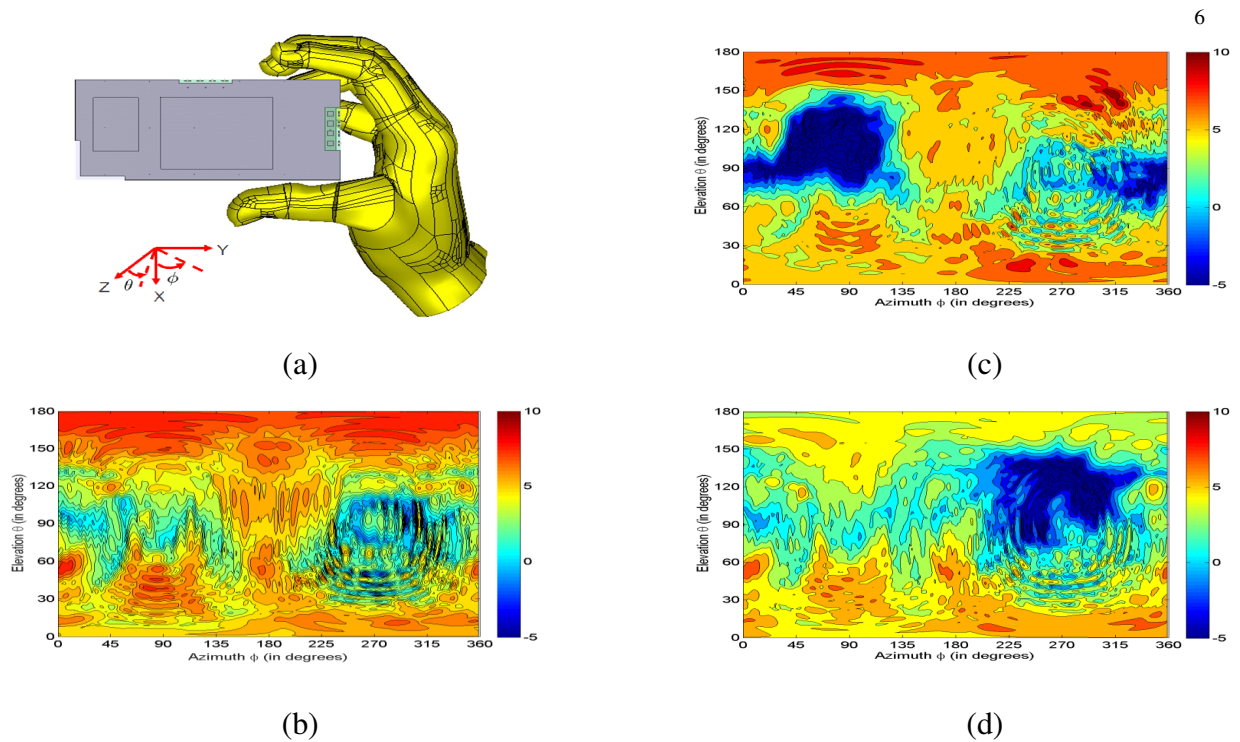


Fig. 1. (a) A typical UE design with multiple subarrays (Top and Long edges) in Landscape mode. Received gain as a function of azimuth and elevation angles for the UE design at 28 GHz in (b) Freespace mode, and with hand blocking in (c) Landscape and (d) Portrait modes.

Furthermore, in the Portrait mode, a blockage region of $120^\circ \times 80^\circ$ (blue areas) is seen and the Long edge subarray does not play an important role in signal reception as it is blocked with the fingers resulting in significantly deteriorated antenna efficiencies. However, the Top edge subarray is not affected much with the presence of the hand. These observations suggest that subarray diversity in UE design is critical in overcoming near-field obstructions as well as to ensure coverage at the UE side over the entire sphere.

Penetration Loss: For the outdoor-to-indoor coverage scenario, material measurements show that penetration loss generally increases with frequency. Further, periodic notches that are several GHz wide and often with more than 30 dB in loss are seen. These losses are attributed to changing material properties with frequency due to which signals constructively/destructively interfere from different surfaces that make the material. While a similar trend is observed across these experiments for both polarizations and different choices of incidence angles, the precise loss at a frequency and the depth of the notches depend on the material, incidence angle and

polarization. This observation motivates the need for designs that support both frequency and spatial diversity.

Path Diversity: Low pre-beamforming signal-to-noise ratios (SNRs) are typically the norm when mm-Wave path losses and additional blockage/penetration losses are incorporated with typical equivalent isotropically radiated power (EIRP) constraints. Thus, a viable system design has to overcome these huge losses with beamforming array gains from the packing of a large number of antennas within the same array aperture [3]–[5], [10]–[13]. In this context, a small number of (at most 4-6) well-spread out (in direction) clusters/paths rendering multi-mode/multi-layer signaling viable are typically observed. The viability of multiple modes suggests the use of both single-user MIMO strategies for increasing the peak rate as well as multi-user MIMO strategies for increasing the sum-rate [11], [14]. Such modes also offer robustness against blockages via intra-base-station beam switching. In addition to the likelihood of multiple viable paths to a certain base-station, there are also viable paths to multiple base-stations. These observations suggest the criticality of a dense deployment of base-stations for robust mm-Wave operation and inter-base-station handover to leverage these paths. Integrated access and backhaul operation is highly desirable for small cell deployment, which also leads to the need to study inter-base-station interference management issues more carefully.

III. EXPERIMENTAL PROTOTYPE DESCRIPTION

Motivated by the system design intuition developed in the previous section, we now describe our experimental prototype system operating in a time-division duplexing framework at 28 GHz. In this setup, baseband analog in-phase and quadrature (IQ) signals are routed to/from the modem to an IQ modulator/demodulator at 2.75 GHz center frequency. The 2.75 GHz intermediate frequency signal is translated to 28 GHz using a 25.25 GHz tunable local oscillator (with a 100 MHz step size). The bandwidth supported is 240 MHz at a sampling rate of 240 Msps. ADCs with an effective number of bits (ENOB) resolution of 8 bits are used at both ends. At the base-station end, the 28 GHz signal is routed to an 16×8 element planar array (a waveguide design) and analog beamforming is applied using tunable four bit phase shifters and gain controllers. The prototype uses a transmit power dynamic range of 19 dB with a maximum EIRP of 55 dBm. As motivated earlier, to overcome blockage, the UE end is made of four selectable subarrays, each a four element phased array of either dipoles or patches as in Fig. 1(a).

With beamforming being a central component in meeting the mm-Wave link budget, RF component and architecture-driven challenges (e.g., cost, power, complexity, form factor, regulatory constraints, etc.) play a principal role in determining practically viable hybrid beamforming solutions. In this context, the *sparse* and *directional* channel structure suggests the use of a certain subset of *directional* beamforming strategies along the dominant clusters/paths at both ends [5], [12]–[14] relative to optimal beamforming along the dominant eigen-modes/singular vectors of the channel matrix. Directional beamforming structures offer robustness to small perturbations in the channel matrix and also allow a tradeoff between peak beamforming gain and initial UE discovery latency (with minimal loss relative to the optimal schemes) via the construction of a hierarchy of directional codebooks [13]. The directional channel structure can be leveraged for scheduling and can also be generalized to multi-user beamforming design with the following solutions: i) beam steering to each UE (with complete agnosticism of the interference caused to other users), ii) zeroforcing (where each user’s beamforming vector steers a beam null to the other users), and iii) generalized eigenvector precoding (that performs a weighted combination of beam steering and beam nulling). These solutions can result in substantial performance improvement over single-user solutions. The readers are referred to [14] for technical details on these constructions as well as performance studies in outdoor and indoor deployments.

Motivated by the robustness of directional beamformers, this solution is implemented in the prototype by leveraging the beam broadening principles described in [13, Sec. IVB] to construct static analog beam codebooks to be used at both the base-station and UE ends. The experimental system implements mm-Wave beamforming by initially determining the best beam direction to be used at either end. After this, the system continuously evaluates all possible beam directions from all available transmitters and switches to the best beam and the best transmitter (handover) with little to no performance degradation. In addition, the system adjusts its parameters to optimize for the link type (LOS/NLOS) by SNR control allowing upto 64-QAM operation.

The seamless beam switching and capability to maintain high SNR enable the experimental system to realize high rates (on both the downlink and uplink) and robustly maintain these rates despite channel variations. That said, the main focus behind the experimental system is *not* the optimization of data-rates, but to study the various fundamental difficulties in realizing mm-Wave systems in practice, especially with NLOS links. In the next two sections, we describe some experimental results illustrating the versatility of the prototype.

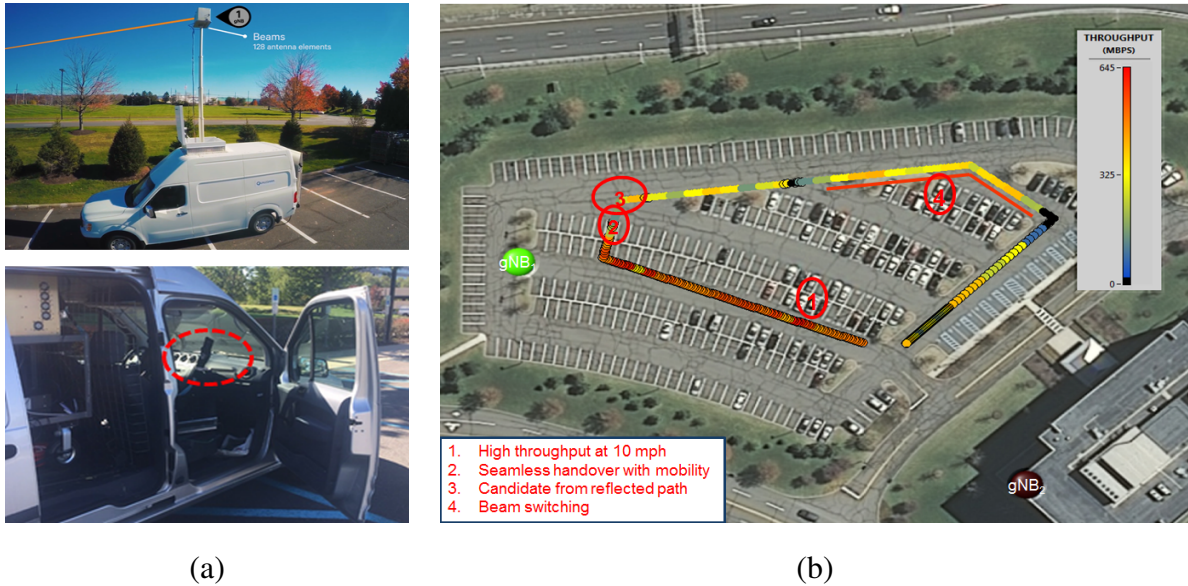


Fig. 2. (a) Elevated gNB and UE inside the testing vehicle used in outdoor testing. (b) Aerial layout of the testing range including gNB locations, achieved rates and important features in rates as the UE is driven over the trajectory.

IV. OUTDOOR MOBILITY STUDIES

An outdoor mobility testing experiment (see Fig. 2(a)) is conducted in the parking spaces adjacent to the Qualcomm building (see aerial layout in Fig. 2(b)). One base-station is mounted on a mast elevated 14 feet in a testing vehicle and located in the parking lot (marked gNB₁), and another base-station is mounted in the sixth floor of the Qualcomm building facing the window and elevated 5 feet from the ground (marked gNB₂). gNB₁ and gNB₂ have a 90° and 110° downtilt, respectively. The UE is mounted on the dashboard of another testing vehicle and testing is done by driving through the parking spaces at 10-15 mph speeds. Fig. 2(b) plots the achieved throughput (in Mbps) as a function of the driving trajectory. From this plot, we note that a high throughput close to 600 Mbps is realized (Scenario 1) when gNB₂ has an unobstructed LOS path to the UE. As the UE moves over the trajectory (Scenario 2), seamless handover is realized between gNB₂ and gNB₁. Further, as the UE is driven on this trajectory, the LOS path from gNB₁ is obstructed and communication is realized through a reflected path first (Scenario 3) and other paths subsequently (Scenario 4) leading to a drop in throughput (gradings in the heat map). This experiment illustrates the prototype's capability to maintain mm-Wave links robustly in outdoor scenarios with intra- and inter-base-station beam switching and handover.

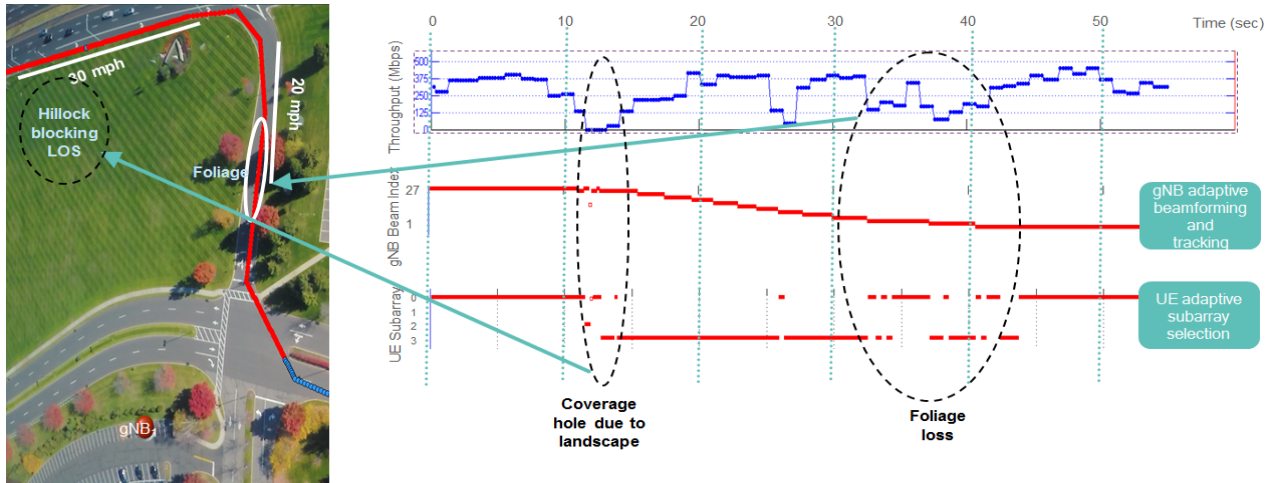


Fig. 3. Left: Outdoor aerial layout of experiment including key geographical features. Right: Achieved rates as a function of outdoor trajectory and time as well as beam indices at gNB and subarray indices at UE.

In a second study illustrated in Fig. 3, an outdoor mobility experiment around the Qualcomm building is conducted. This environment is mostly a tree-lined open square-type setting with some street canyon-type features. Specific points-of-interest include parking lots and structures with bordering buildings having glass window panes, foliage (a mix of pine and spruce trees), a large shopping mall in close vicinity (Bridgewater Commons Mall), highways (US Rt. 202), etc. For the specific experiment reported here, a testing vehicle is driven for a period of ≈ 55 seconds through the exit lane of US Rt. 202 at a speed of 20-30 mph, onto the ramp and into a side street enveloping the Qualcomm building (see trajectory in red in Fig. 3, Left side). In terms of notable observations from this experiment, a base-station mounted on a raised platform at 24 feet with a 90° downtilt (marked gNB₁) offers a LOS path to the UE as it starts exiting from Rt. 202 (throughput of 375 Mbps). However, as the UE traverses the exit lane, a small hillock-like feature blocks the LOS path leading to a coverage hole that cannot be bridged with any reasonable NLOS path from this base-station and a significant deterioration in rate. This observation points at the necessity of sufficient base-station density to enhance mm-Wave coverage under blockages. For example, a base-station on the opposite side of the highway (Rt. 202) could have provided coverage to the UE over this coverage hole. As the UE crosses this feature, a beam recovery process recovers the LOS path albeit with a different subarray offering complementary coverage

in the LOS direction leading to an improved throughput of 375 Mbps. Further, as the testing vehicle enters the ramp, blockage loss due to foliage results in a throughput drop (125-250 Mbps) and two subarrays turn out to be useful over this period. As the UE exits the ramp onto the adjoining street, the LOS path is recovered leading to a throughput of over 375 Mbps. The distance between the gNB and UE varies from 50-100 m over the whole experiment.

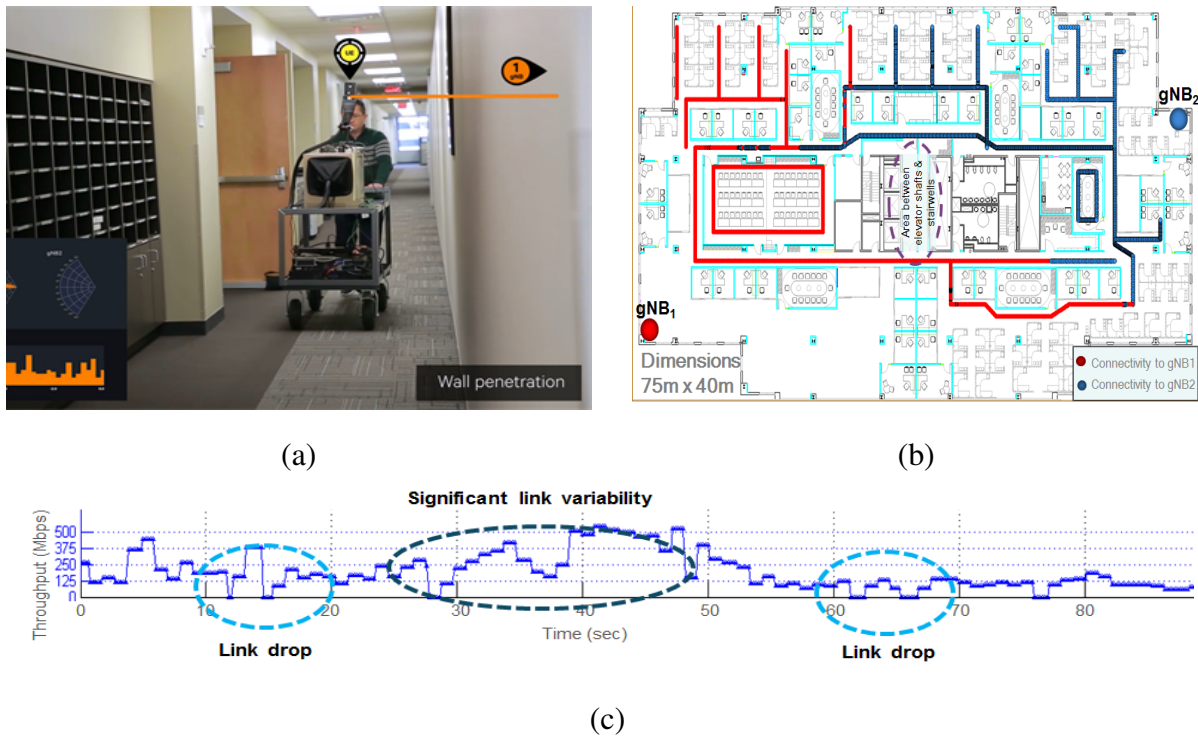


Fig. 4. (a) Typical UE testing with pedestrian mobility in an indoor scenario. (b) Indoor layout and building plan along with two gNB locations and coverage areas. (c) Achieved rate along with key features in the rate trajectory over a certain indoor segment.

V. INDOOR MOBILITY STUDIES

Complementary to the above discussion, an indoor mobility study (see Fig. 4(a)) in the third floor of the Qualcomm building (see building layout in Fig. 4(b)) is now described. The floor plan is mostly comprised of cubicles along the edge with walled offices and conference rooms towards the center. Two base-stations (marked gNB₁ and gNB₂) are placed at the far corners of the floor plan and the UE is moved at pedestrian speeds through the layout. From our studies, these two base-stations are sufficient to guarantee adequate coverage with at least 1 bps/Hz

spectral efficiency as the UE is traversed through the floor plan (coverage areas with each gNB marked in red and blue of Fig. 4(b), respectively). Nevertheless, the coverage area corresponding to each gNB does not lead to a well-defined cell boundary and is clearly dependent on the environment, material properties, etc. This observation points to necessity of further system coverage studies with irregular cell boundaries and base-station density to overcome coverage holes in such scenarios. As a particular illustration of this study, the throughput achieved with an ≈ 90 second trajectory is illustrated in Fig. 4(c) which illustrates both link drops due to penetration loss through obstructions (concrete, elevator area, wall, metallic material, etc.) and link variability due to changing material properties. Such link drops can be mitigated with enhanced beamforming, fast subarray switching, network densification, etc.

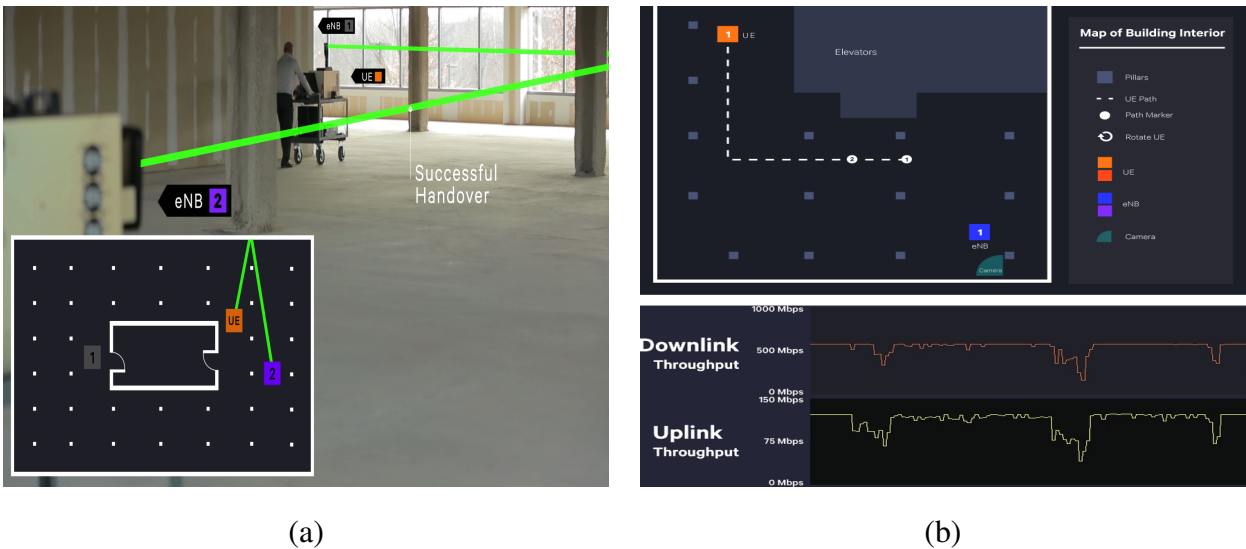


Fig. 5. (a) A successful handover from eNB_1 to eNB_2 in an indoor setup. (b) Layout of another indoor coverage experiment with downlink/uplink rates using the proposed beamforming solutions.

More indoor mobility experiments can be seen in the video demonstration at [15]. In one experiment, illustrated in Fig. 5(a) and seen in [15], a LOS link is initially established between the transmitter (labeled eNB_1) and receiver (labeled UE) by beam scanning at both ends. With a high SNR from the LOS link, a high rate is established on both the downlink and uplink. As the UE is moved across the long edge of the hallway (see relative positions of eNB_1 , eNB_2 and UE in the bottom left inset of Fig. 5(a)), the link connecting eNB_1 with the UE becomes NLOS with increasing path loss as the distance between eNB_1 and UE increases. As the UE turns the corner

at the short edge, the NLOS¹ link between eNB₂ and UE becomes better than the NLOS link between eNB₁ and UE and a successful handover (illustrating robustness to blockage) happens from eNB₁ to eNB₂, as shown in Fig. 5(a).

Figure 5(b) illustrates the layout of yet another indoor experiment where the UE is moved from an initial position (marked “1” in a white circle) towards its final destination (marked “1” in an orange square) via the dashed white-line trajectory. As the UE is moved over the trajectory, the achieved downlink and uplink rates show many disruptions as the connected path is blocked by the pillars in the layout (marked as gray squares). For example, when the pillar blocks the LOS path, connection is established to the dominant NLOS path (again through reflections) leading to the first disruption in rate(s). Connection is re-established to the LOS path as the UE moves past the pillar until the next pillar is reached where the second disruption happens. The third disruption corresponds to the switch from the re-established LOS path to the dominant NLOS path as the UE turns the corner. Thus, these examples illustrate the robustness of our proposed beamforming solutions to blockages in real deployments.

VI. CONCLUDING REMARKS

A. Summary

This article provides a brief overview of mm-Wave channel measurements and what the implications of these measurements are for system design. An immediate consequence of the blockage and penetration losses inherent and specific to mm-Wave systems are the poor link margins. These motivate the necessity to reap spatial array gains via the use of near-optimal beamforming solutions over large antenna arrays. Prominent challenges in this goal include the limited range and performance of mm-Wave components, as well as the robustness of the beamforming solution to spatio-temporal channel variations and its impact on overall system design. Further, cost considerations may allow only the use of a small number of RF chains at either end and thus the beamforming solutions should be adaptive to changes in the RF architecture(s). Towards this goal, directional beamforming approaches can be used as robust, low-complexity, near-optimal solutions that help overcome the high propagation losses at mm-Wave frequencies. Such solutions are demonstrated with our experimental prototype, illustrating

¹Note that the LOS link between eNB₂ and UE is blocked by a pillar in the layout, all marked in white squares.

the viability of mm-Wave systems for high data-rate requirements. In particular, the prototype system demonstrates: i) beamforming and beam scanning, ii) outdoor coverage and mobility, iii) resilience to blockage of paths, iv) inter-base-station handover, v) indoor mobility, and vi) interference management in both outdoor and indoor settings.

B. Future Research Directions

Important issues that require further study include: i) a more exhaustive study on realistic channel modeling for mm-Wave propagation, ii) models for spatio-temporal channel variations, iii) models for impairments such as hand/body/human blockages, phase noise, etc., iv) advanced MIMO techniques for both single- and multi-user multi-carrier transmissions, v) impact of mm-Wave channel properties on mm-Wave system/network design issues such as coverage and network latency tradeoffs, mm-Wave handover, interworking with sub-6 GHz bands and applications, integrated access-backhaul solutions, vi) advanced MIMO RF architectures such as [5]–[8] for prototype studies and real deployments, vii) RF tradeoffs in form factor UE design, etc.

REFERENCES

- [1] F. Boccardi *et al.*, “Five disruptive technology directions for 5G,” *IEEE Commun. Magaz.*, vol. 52, no. 2, Feb. 2014, pp. 74–80.
- [2] T. S. Rappaport *et al.*, “Millimeter wave mobile communications for 5G cellular: It will work!,” *IEEE Access*, vol. 1, 2013, pp. 335–349.
- [3] R. W. Heath, Jr. *et al.*, “An overview of signal processing techniques for millimeter wave MIMO systems,” *IEEE Journ. Sel. Topics in Sig. Proc.*, vol. 10, no. 3, Apr. 2016, pp. 436–453.
- [4] W. Roh *et al.*, “Millimeter-wave beamforming as an enabling technology for 5G cellular communications: Theoretical feasibility and prototype results,” *IEEE Commun. Magaz.*, vol. 52, no. 2, Feb. 2014, pp. 106–113.
- [5] J. Brady, N. Behdad, and A. M. Sayeed, “Beamspace MIMO for millimeter-wave communications: System architecture, modeling, analysis and measurements,” *IEEE Trans. Ant. Propagat.*, vol. 61, no. 7, July 2013, pp. 3814–3827.
- [6] Y. Zeng and R. Zhang, “Millimeter wave MIMO with lens antenna array: A new path division multiplexing paradigm,” *IEEE Trans. Commun.*, vol. 64, no. 4, Apr. 2016, pp. 1557–1571.
- [7] J. A. Laurinaho *et al.*, “2-D beam-steerable integrated lens antenna system for 5G E-band access and backhaul,” *IEEE Trans. on Microwave Theory and Tech.*, vol. 64, no. 7, July 2016, pp. 2244–2255.
- [8] T. Kwon *et al.*, “RF lens-embedded massive MIMO systems: Fabrication issues and codebook design,” *IEEE Trans. on Microwave Theory and Tech.*, vol. 64, no. 7, July 2016, pp. 2256–2271.
- [9] V. Raghavan *et al.*, “Millimeter wave channel measurements and implications for PHY layer design,” *IEEE Trans. Ant. Propagat.*, vol. 65, no. 12, Dec. 2017.

- [10] S. Hur *et al.*, “Millimeter wave beamforming for wireless backhaul and access in small cell networks,” *IEEE Trans. Commun.*, vol. 61, no. 10, Oct. 2014, pp. 4391–4403.
- [11] S. Sun *et al.*, “MIMO for millimeter wave wireless communications: Beamforming, spatial multiplexing, or both?,” *IEEE Commun. Magaz.*, vol. 52, no. 12, Dec. 2014, pp. 110–121.
- [12] O. El Ayach *et al.*, “Spatially sparse precoding in millimeter wave MIMO systems,” *IEEE Trans. Wireless Commun.*, vol. 13, no. 3, Mar. 2014, pp. 1499–1513.
- [13] V. Raghavan *et al.*, “Beamforming tradeoffs for initial UE discovery in millimeter-wave MIMO systems,” *IEEE Journ. Sel. Topics in Sig. Proc.*, vol. 10, no. 3, Apr. 2016, pp. 543–559.
- [14] V. Raghavan *et al.*, “Single-user vs. multi-user precoding for millimeter wave MIMO systems,” *IEEE Journ. Sel. Areas in Commun.*, vol. 35, no. 6, June 2017, pp. 1387–1401.
- [15] Qualcomm, “5G mm-Wave demonstration,” <https://www.qualcomm.com/videos/5g-mmwave-demonstration>, Accessed on Sept. 29, 2017.